Experimental and Numerical Investigation on Compression Orthotropic Properties of Spruce Wood in Axial and Transverse Loading Directions

Weizhou ZHONG[1], Alexis RUSINEK[2], Tomasz JANKOWIAK[3], Xicheng HUANG[1], Farid ABED[4]

[1] *Institute of Systems Engineering*
China Academy of Engineering Physics
P.O.Box 919-401 621999, Mianyang, Sichuan, China
e-mail: {zhongwz, huangxc}@caep.cn

[2] *National Engineering School of Metz,*
Laboratory of Mechanics, Biomechanics, Polymers and Structures
1 route d'Ars Laquenexy, CS 65820 57078 Metz Cedex 3, France
e-mail: rusinek@enim.fr

[3] *Institute of Structural Engineering*
Poznan University of Technology
Piotrowo 5, 60-965 Poznan, Poland
e-mail: tomasz.jankowiak@put.poznan.pl

[4] *Department of Civil Engineering*
American University of Sharjah
P.O.Box 26666 Sharjah, U.A.E.
e-mail: fabed@aus.edu

Compression tests on spruce wood in axial, radial and tangential directions have been performed using an INSTRON hydraulic machine. Spruce elastic mechanical properties and plastic deformation behaviour are presented. Experimental results allow to demonstrate different spruce failure modes: fibers buckling and collapsing are noticed under axial compression whereas, fibers slippage and delamination are the main failure modes under compression loading in radial and tangential directions. Spruce energy absorption efficiency and ideality energy absorption efficiency in the three loading directions are also analyzed. Representative volume element (RVE) model is adopted assuming transverse isotropic behavior to simulate wood microstructure in all directions. It was shown that micro-cell arrangement leads to wood macromechanical property spatial anisotropy. Porosity and hole shape effects on simulation results are estimated by RVE models with hexagon, circle, pentagon and square holes.

Key words: spruce wood, orthotropic, energy absorption, representative volume element, numerical simulation.

1. Introduction

Wood cell tissue parallel to growth orientation shows different mechanical responses depending on axial, radial and tangential loading directions. Compressive stress plateau may extend up to a 60% deformation. So wood is often used as an impact limiter in containers for nuclear wastes transportation and in blast loading protection systems [1]. Wood goes through elastic, yield plateau and compaction phases during compression loading. Linear elasticity is usually assumed to describe the initial small deformation. A wide stress plateau appears next in the compressive stress-strain curve which is caused by a gradual fibers buckling and breakage in wood cells. In compaction phase, the stress increases noticeably when the wood cells are fully compacted.

The mechanical behavior of wood is highly influenced by the response of its internal microstructure. Recently many advanced microscope apparatuses are adopted to observe wood cell microstructure. TRTIK *et al.* [2] applied synchrotron radiation phase-contrast X-ray tomographic microscopy to observe the features of spruce anatomy at the cellular length scale. The experiments clearly revealed spruce heartwood characteristics. GINDL *et al.* [3] performed nanoindentation experiments and analyzed spruce microfibril angle and lignin content. The relationship between wood deformation and the nanostructure was investigated using small-angle X-ray scattering by REITERER [4]. Based on the modern experimental technique, elastic modulus and bending behavior of wood were also investigated in the literatures [5–7].

As a natural species, the mechanical properties of wood are highly affected by moisture content, strain rate and temperature. Many experimental studies focused on examining the effect of these factors on macro-mechanical properties of wood. For example, VURAL and WIDEHAMMAR [8, 9] investigated strain rate relativity of wood behavior using a revised split Hopkinson pressure bar. GINDL [10] indicated that lignin moisture has an obvious influence on wood axial compression property, where a reduction of lignin content in standing trees leads to a decrease of compressive strength and a diminished modulus of elasticity. GONG [11] investigated failure mechanisms of air-dried black spruce under axial compression condition by polarised-light microscopy. YILDIZ [12] examined the heat treatment effects on spruce compression strength. The experimental results showed that wood properties are affected greatly by humidity, loading velocity and temperature environment.

Numerical simulation is an economic and convenient approach in material and structure mechanics research. It is an effective supplement for theoretical and experimental investigation of material behavior. In recent years, finite element analysis has been used to simulate wood's mechanical response by some researchers. SAAVEDRA FLORES [13] proposed a fully coupled multi-scale finite

element model for constitutive description of wood cell wall. Vasic [14] introduced some numerical models for wood fracture failure and explored avenues toward achieving wood fracture models. Taking the complexity of wood's microstructure into account, some simplified finite element models and material constitutive relations have also been adopted in numerical simulation [15, 16].

Wood, as an orthotropic material, shows different cushion properties in axial and transverse loading directions. Although wood and wood-like material mechanical properties and failure mechanism in axial direction were investigated by many researchers [17–22], wood transverse compression deformation properties are little mentioned. In the present work, quasi-static compression tests are performed in axial, radial and tangential directions of spruce wood using a hydraulic machine. The corresponding stress strain relationships are presented and energy absorption efficiency in different loading directions is analyzed. Finite element (FE) analysis is also conducted by modeling representative volume elements from the spruce microstructure to simulate anisotropic behavior under axial and transverse compression conditions.

2. Compression mechanical properties of spruce wood

Spruce specimens were cut from a 610 mm diameter trunk with moisture content close to 12.72% and a density equal to 413 kg/m^3. Uniaxial compression tests were performed using an INSTRON hydraulic machine. Loadings along the three perpendicular directions: axial, tangential and radial were considered, see Fig. 1. The specimens were cut taking into consideration wood growing direction and annual rings [18]. Axial is consistent with wood growth direction, radial is orthogonal to annual ring and tangential is tangent to annual ring in long grained section.
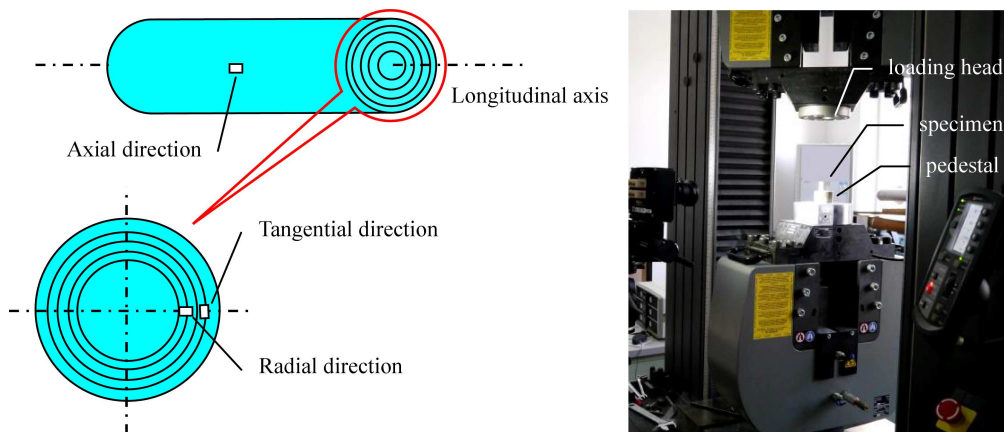
Fig. 1. Schematic description of wood material directions and experimental machine.

Cuboid specimens with $30 \times 2 \times 20$ mm edge dimensions were used in this experimental study. For axial compression specimen, the 30 mm side was taken along the tree growth direction. The largest edge was orthogonal or tangent to annual ring for radial and tangential compression specimens, respectively. In other word, loading direction during the experiments was parallel to the largest edge. All tests were conducted at room temperature under a constant strain rate equal to 10^{-3} s^{-1}. An extensometer was attached to the specimen for accurate strain measurement and elastic modulus calculation. For comparison convenience, and taking into consideration the wood compressibility, engineering stresses and strains are considered in the present descriptions of experimental and FE results. Samples of the compressive stress-strain curves at the elastic zones along axial, radial and tangential directions are presented in Fig. 2. The calculated axial, radial and tangential elastic moduli were 11331 MPa, 532 MPa and 351 MPa, respectively.
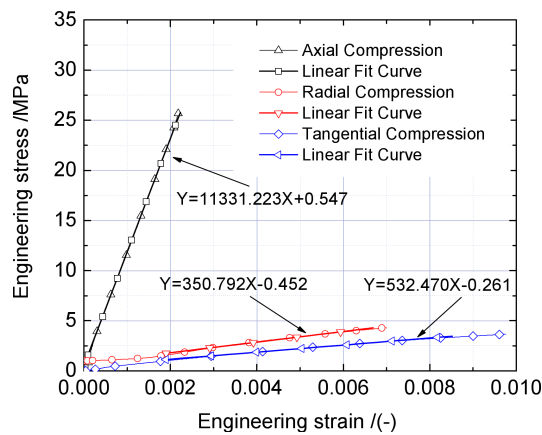
FIG. 2. Young modulus values depending on different loading directions.

The complete stress strain curves for several samples that were tested under different loading directions are illustrated in Fig. 3. It is obvious that spruce specimen goes through elastic, yield plateau and compact phases during compression process. Plastic deformations occurred at strains equal to 8%, 4.7%, and 4.5% for axial, radial and tangential loading directions, respectively. The corresponding yield stresses were measured as 37.8 MPa, 4.42 MPa, and 4.40 MPa, respectively. In the yield plateau phase, the compressive stress decreases with plastic straining under axial deformation, whereas it slightly increases under radial deformation and almost constant for the case of tangential loading. In all cases, a significant and rapid increase in the compressive stresses is observed at around 60% strains, a stage referred to as the compaction phase. The large stresses recorded during the compaction phase may be attributed to the fact
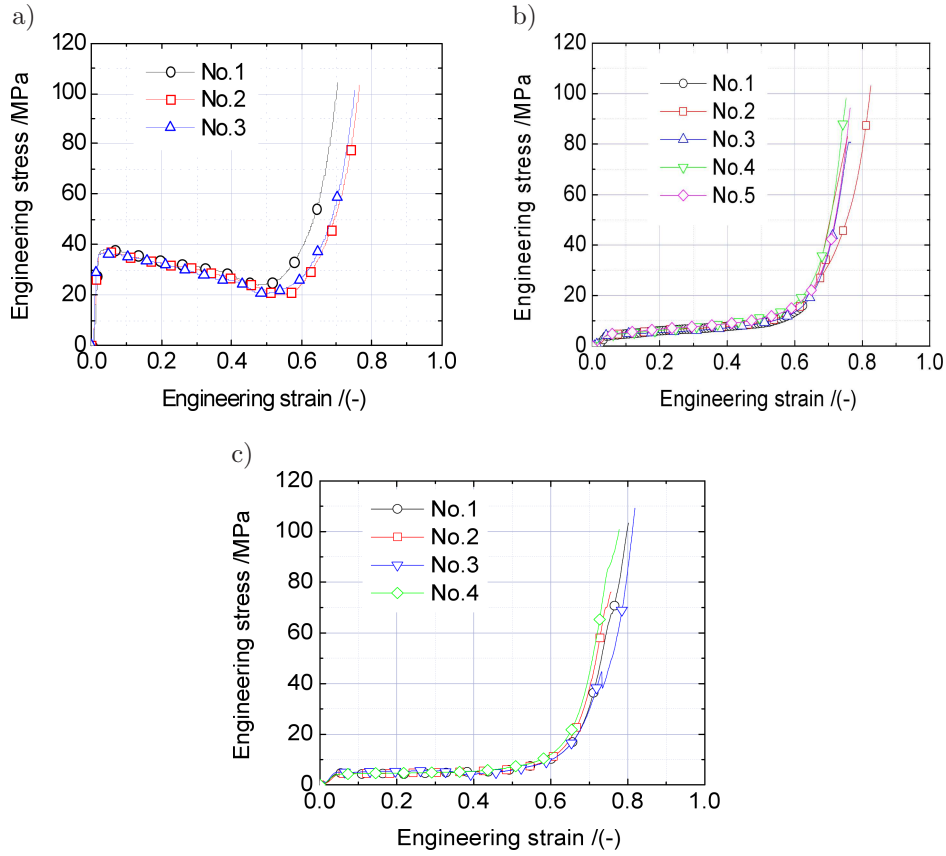
FIG. 3. Stress versus strain curves for different compression directions:
a) axial, b) radial, c) tangential.

that the spruce cell walls are collapsed and the porous wood specimen was fully compressed into a rigid piece.

Figure 4 shows samples of the failures modes for different loading directions and at different loading stages. Buckling and collapse taking place during plastic
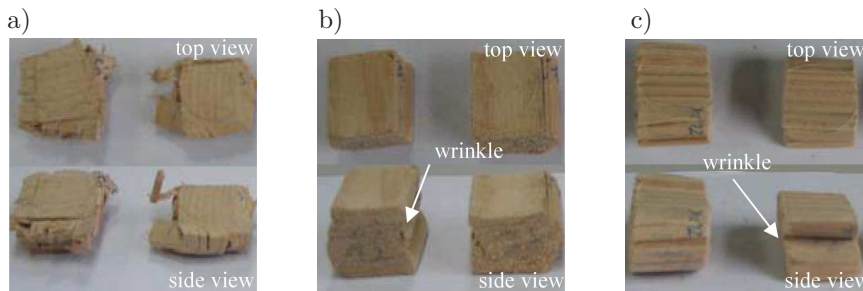
FIG. 4. Failure modes for specimens tested under a) axial, b) radial
and c) tangential compressions.

deformation increasing process was the dominant failure mode for the case of axial loading, which explains the decrease in compressive stresses in the yielding stage. On the other hand, the failure mode for specimens under radial and tangential compressive loadings was mainly controlled by fiber slippage and delamination.

3. Energy absorption for each loading directions

Material energy absorption can be calculated based on the stress strain results as follows:

$$(3.1) \qquad W = \int_{0}^{\varepsilon_m} \sigma \, d\varepsilon,$$

where σ and ε are stress and strain, respectively during loading process, and ε_m is strain at the maximum stress level σ_m.

Energy absorption efficiency (E) and ideality energy absorption efficiency (I) are used to describe absorption capacity of porous foam materials. These two energy indices are expressed in terms of the stress strain results where E is defined as the ratio of total energy density (toughness) to the maximum stress as given by Eq. (3.2), whereas ideality is defined as the ratio of material toughness to the product of maximum stress and maximum strain as given in Eq. (3.3), [22]:

$$(3.2) \qquad E = \frac{\displaystyle\int_{0}^{\varepsilon_m} \sigma \, d\varepsilon}{\sigma_m},$$

$$(3.3) \qquad I = \frac{\displaystyle\int_{0}^{\varepsilon_m} \sigma \, d\varepsilon}{\sigma_m \varepsilon_m}.$$

As spruce is a cellular material, its energy absorption evaluation per unit volume ($1\times1\times1$ m) can be computed using the above three equations. Based on the experimental stress strain results given in Fig. 3, spruce unit volume energy absorptions in axial, radial and tangential directions are calculated and presented in Fig. 5. It is clear that energy absorption capacity increases with strain. Wood specimen tested under axial compression observed larger stresses and, therefore, has the largest energy absorption capacity as compared to the
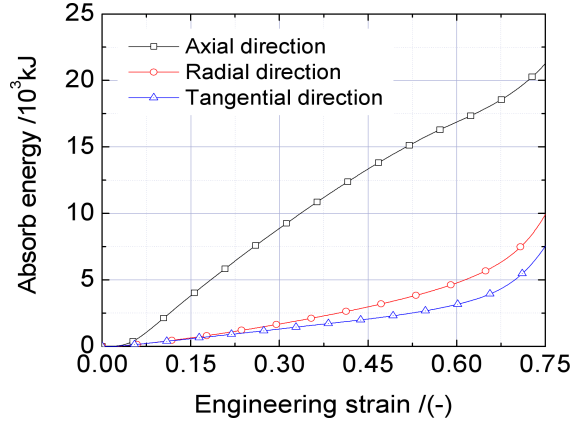
FIG. 5. Energy absorption versus strain curves by unit volume ($1\times1\times1$ m).

energy absorption capacities under radial and tangential loadings. Radial energy absorption capacity is slightly larger than that of tangential direction.

Spruce energy absorption efficiencies calculated using Eq. (3.2) in the three directions are also compared as illustrated in Fig. 6a. At 20% strain or less, energy absorption efficiency curves in the three orthogonal directions are almost identical. Axial energy absorption efficiency becomes larger than the other two at higher strains. Radial energy absorption efficiency is the smallest among the three curves.

Figure 6b shows ideality energy absorption efficiency in the three loading directions. Radial and tangential ideality energy absorption efficiencies are larger than that of axial direction when strain is less than 0.15. When strain is over 0.25,
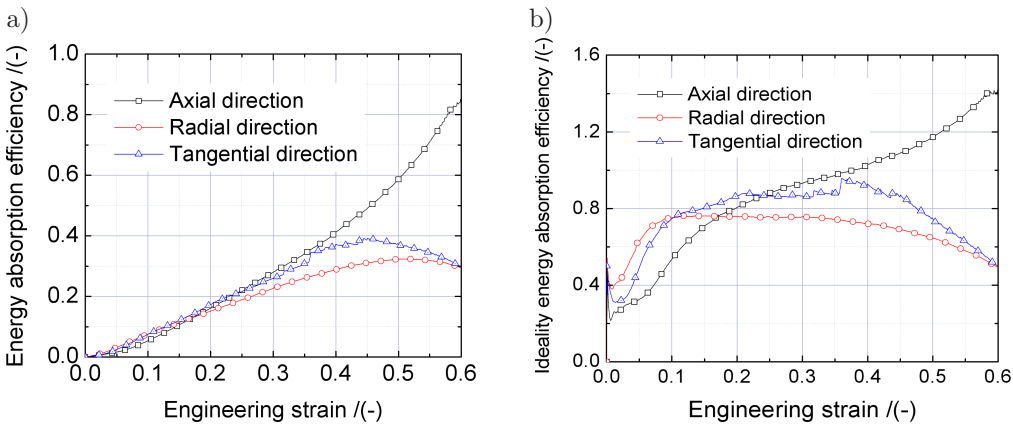
FIG. 6. Energy absorption analysis: a) energy absorption efficiency,
b) ideality energy absorption efficiency.

axial ideality energy absorption efficiency becomes the largest. As axial compression stress versus strain curve is non-monotone, it induces that ideality energy absorption is over 1.0 by Eq. (3.3). Based on the above-mentioned results, it can be concluded that spruce energy absorption efficiencies vary with loading directions. In a wood crash box, rational wood pattern and arrangement in structure brings better cushion energy absorption.

4. MODELING AND NUMERICAL SIMULATION OF SPRUCE MECHANICAL BEHAVIOR

As a porous structure material, wood micro-cellar structure arrangement leads to macroscopic mechanical properties anisotropy. Many rectangle, oval and polygon holes can be found in spruce microstructure by scanning electron microscope as shown in Fig. 7 [8]. It shows that the smallest cell size is about 15 μm and the biggest is about 60 μm. Taking all the hole shapes into account, a simplified hexagonal holes are adopted to representative approximately spruce microstructure in the following simulations. According to the cell dimensions, a representative volume element (RVE) is taken from wood structure to analyze its mechanical behavior. Because the difference of wood yield stresses in radial and tangential directions are small, its material definition can be assumed as transverse isotropy in simplified theory analysis and numerical simulation.

a)   b)
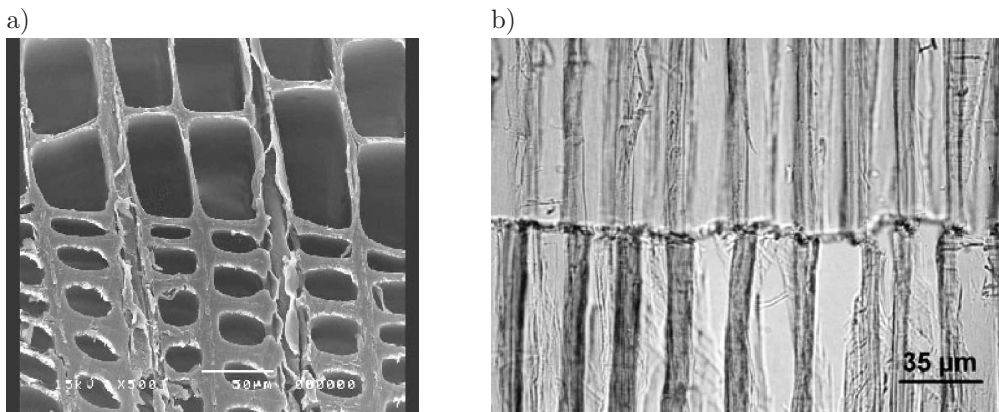
FIG. 7. Scanning electron micrographs: a) cross section, b) tangential section [8].

4.1. RVE model building of spruce microstructure

A wood numerical model with a periodic structural arrangement is adopted in the present numerical simulations. In order to analyze how model dimensions affect simulation results, four cubic models with a side dimension equal 175 μm, 350 μm, 700 μm and 1400 μm are considered as shown in Fig. 8. It is evident
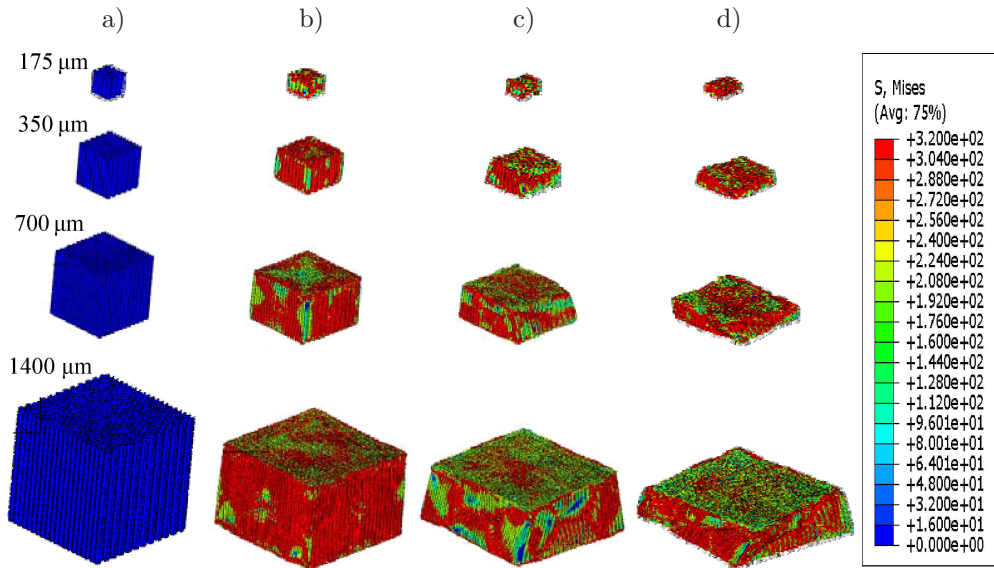
FIG. 8. Scale effect on mechanical behavior under compression:
a) undeformed specimen, b) $\varepsilon = 0.25$, c) $\varepsilon = 0.50$, d) $\varepsilon = 0.75$.

from the deformation processes presented in Fig. 8 that the contours of Misses stresses are not influenced by the model dimension.

The compressive stress strain curves predicted using the FE models showed similar results for the four different models as illustrated in Fig. 9. Stresses at the plateau region deviate a bit with model size. The stress plateau for 175 µm model is the smallest among the other configurations. Stress plateau is nearly consistent when model size is from 350 µm to 1400 µm. It can be concluded
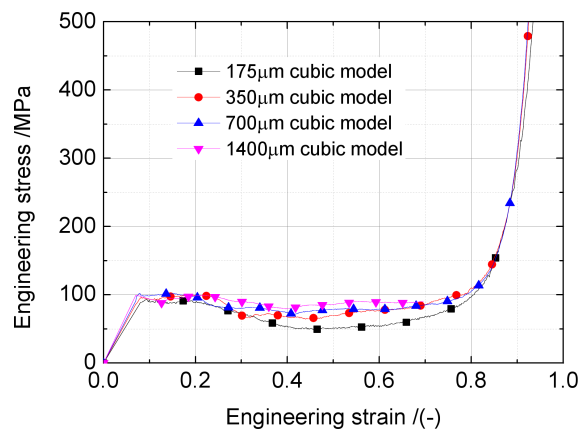
FIG. 9. Mechanical behavior description for different size model.

that model dimension doesn't affect numerical simulation results if numerical model is large enough. Representative volume element model can, therefore, be used to simulate the mechanical behavior of a periodic structure. It is a way to save time after numerical validation to evaluate the mechanical behavior of wood extensively.

Next, a simplified representative volume element model is established to analyze the compression behavior under axial and transverse loading conditions. The detailed dimensions of wood microstructure used in the FE model are shown in Fig. 10. The length of the cubic model is 425 μm and the porosity of wood microstructure is 73.27% for regular hexagon holes arrangement case. Finite element software ABAQUS is adopted to simulate spruce compression behavior using the representative volume element model. The numerical model includes over 250000 nodes and 170000 hexahedral elements (C3D8R Abaqus type). For wood cell wall structure, three major chemical constituents of cellulose, hemicellulose and lignin are contained. Cellulose mass fraction varies from 40–50% in weight of wood substance. Hemicellulose is 15–25% and lignin is 15–30% respectively [23]. So the equivalent mechanical property parameters of spruce cell wall tissue can be calculated shown in Table 1.
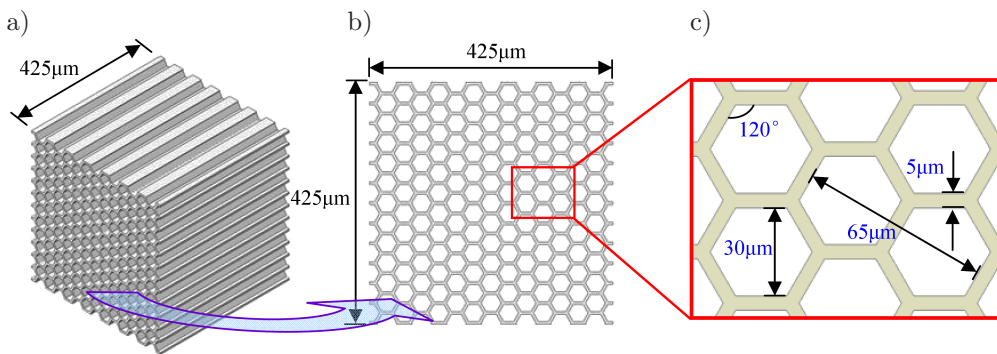
FIG. 10. Dimensions of wood microstructure model using regular hexagon holes: a) 3-D model, b) surface with holes, c) cell description.

Table 1. Mechanical properties of spruce microstructure tissue.

Material	Density [kg/m^3]	Young's modulus [GPa]	Poisson's ratio
spruce	1490	5.84	0.4

4.2. Numerical simulation of axial compression behavior

Spruce microstructure mechanical behavior under axial compression is simulated. A constant velocity of 5 m/s is applied during the loading process. Compressive stress stain curve shown in Fig. 11 clearly shows three phases in axial
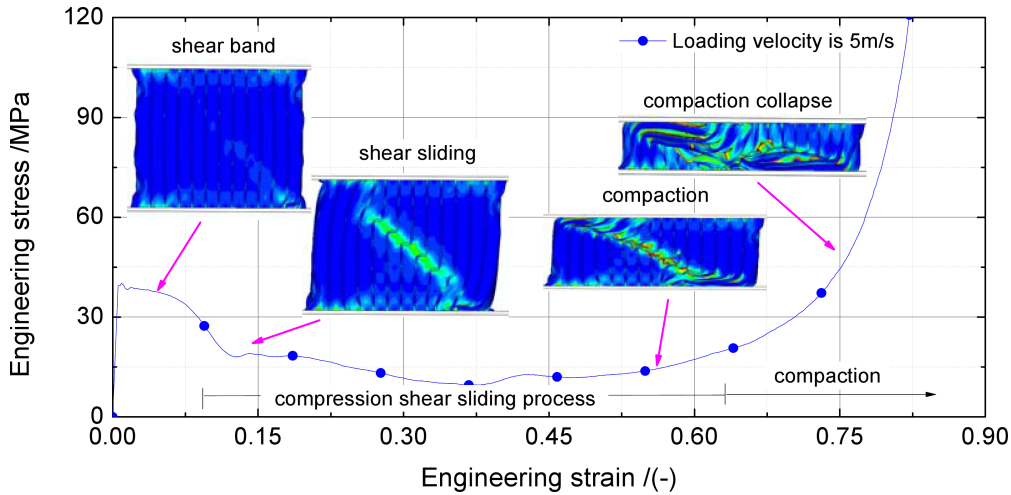
FIG. 11. Axial compression stress versus strain curve for $v_0 = 5$ m/s.

compression process. Firstly wood goes through short linear elastic deformation. Then a shear band occurs in wood microstructure. The angle between shear band and loading direction is about 45°. Stress decreases when strain increases from 0.01 to 0.12. With strain increasing over 0.12, stress turns into a wide stable phase, indicating a gradual shear sliding. Wood enters into compaction phase when strain reaches about 0.6 at which a significant increase in stress is observed.

Detailed deformation process of spruce microstructure is shown in Fig. 12. Shear sliding along 45° direction is the main failure mode for wood microstructure under axial compression. Buckling occurs on side cell wall as shown in
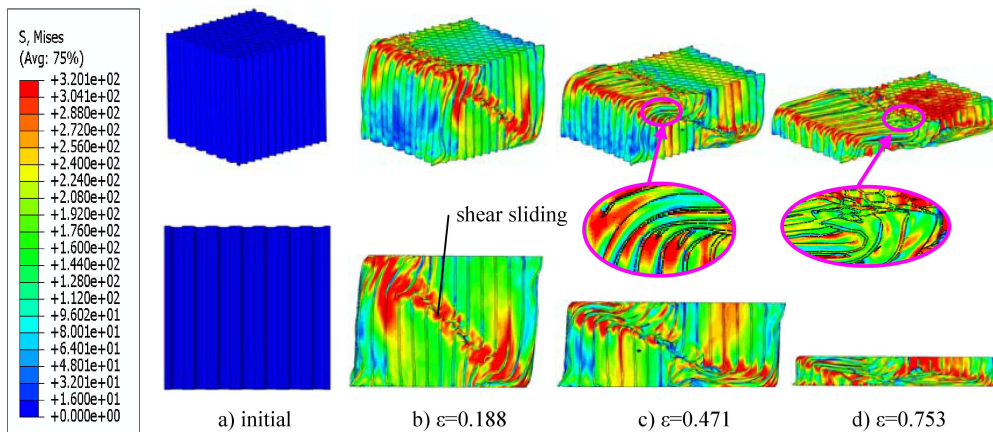
FIG. 12. Axial compression collapse process of wood microstructure for $v_0 = 5$ m/s.

Fig. 12d. It can be seen that the main energy dissipation modes of axial compression are cell wall shear sliding and collapse. Buckling and collapse phenomena occur usually in wood under axial compression. It induces that compression stress changes greatly at initial yield position as illustrated in Fig. 11.

4.3. Numerical simulation on transverse compression behavior

In order to analyze wood mechanical property in the transverse direction, compression response of spruce microstructure under transverse displacement velocity of 5 m/s is considered. The corresponding stress strain curve along the transverse direction is given in Fig. 13. Due to wood cell arrangement pattern, the mechanical property under transverse compression loading is found to be like most foam materials. The typical three phases of linear elastic deformation, stable stress plateau and compaction process are very obvious. Transverse plateau stress is about 9 MPa which is much less than that of axial loading. Several 45° shear bands and hexagonal cell wall collapses occurred gradually in transverse compression process. When strain reaches 0.66, the wood structure was compressed completely and stress increases quickly.
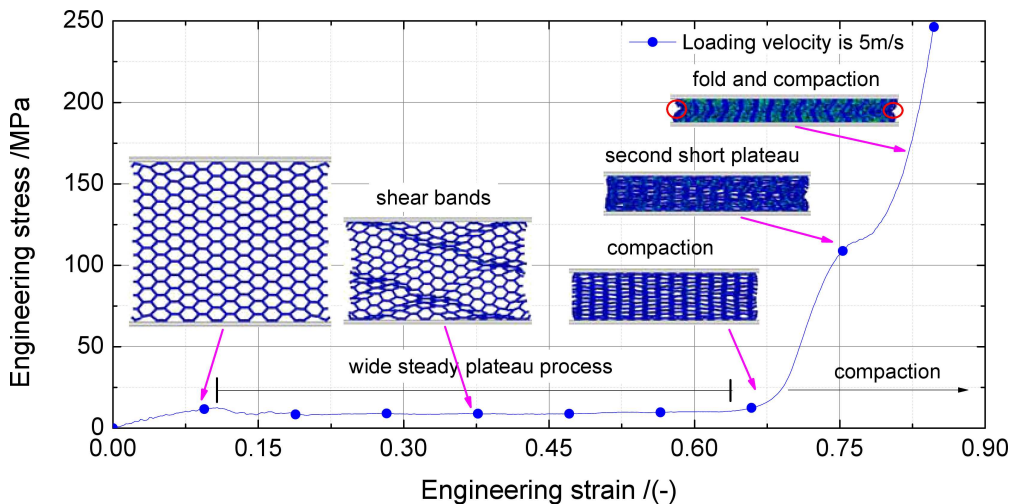
FIG. 13. Transverse compression stress versus strain curve for $v_0 = 5$ m/s.

Being different from axial compression, deformation process of transverse loading is more stable. The main failure mode was shear bands leading to a gradual collapse as shown in Fig. 14. Deformation distribution of spruce microstructure was uniform until finally compressed into a flat. For transverse compression condition, plastic fold of wood cell is the main energy dissipation mode as marked by ellipse in Fig. 14. Lateral deformation is tiny during plastic plateau stress
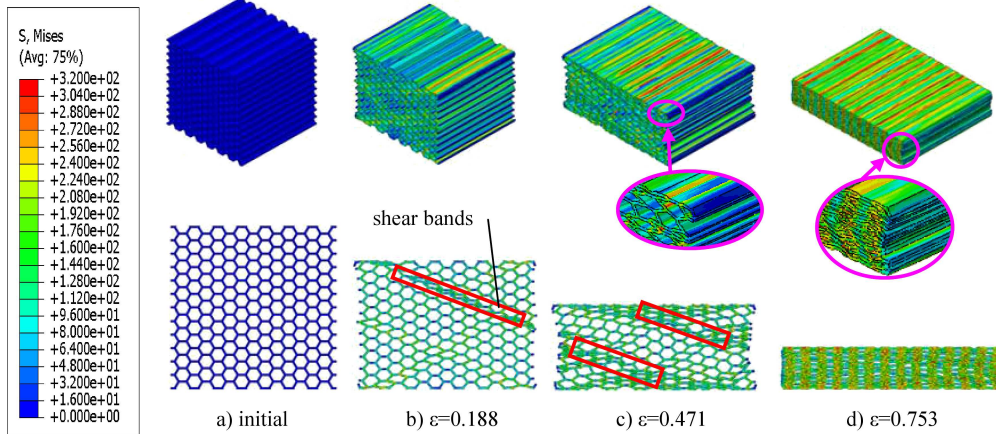
FIG. 14. Transverse compression collapse process of wood microstructure for $v_0 = 5$ m/s.

phase, so wood can be approximately taken as a compressible material when deformation is below the locked strain value.

4.4. FE stress strain comparisons with experiments

Comparison of stress strain curves under axial compression between numerical simulation and experimental results is shown in Fig. 15. It can be seen that the two curves have similar trends, with slight variation in stresses along the plateau region. As spruce wood belongs to fast-growing coniferous species, water and pits are always presented inside the cell wood. Many local defects usually exist in wood microstructure, too. However, the effect of water and
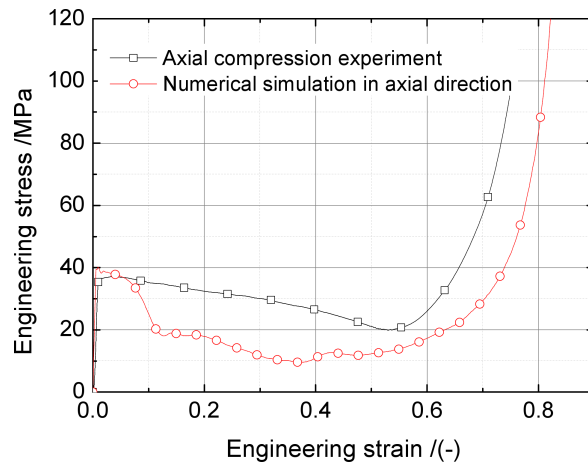
FIG. 15. Experimental and numerical comparison under axial compression.

pit were ignored in the simplified numerical model. This may explain the high FE stress values along the plateau region as compared to their experimental counterparts. Nevertheless, the curve growing trends predicted numerically are consistent with experimental observations. It indicates that the present simplified numerical model is effective partly to simulate large deformation behavior for wood.

The stress strain curve predicted numerically under transverse compression loading is also compared with the experimental results under radial and tangential compressions as shown in Fig. 16. No significant difference was observed among the three curves. It indicates that the simplification of using transversely isotropic FE model is valid for wood mechanical behavior description. Unlike the case of axial compression, radial and tangential compression deformation processes are much smoother. Stress is monotonically increasing in transverse compression process. On the contrary, axial compression stress decrease abruptly in the early stage of plateau stress as discussed earlier in Fig. 15. Buckling and collapse of cell wall result in axial compressive instability. Plastic deformation is not uniform under axial compression condition. Wood cell wall is compressed uniformly and gradually in radial or tangential compression. Though axial compression is with greater energy dissipation, stability and controllability of radial and tangential loading are more superior to axial compression case.
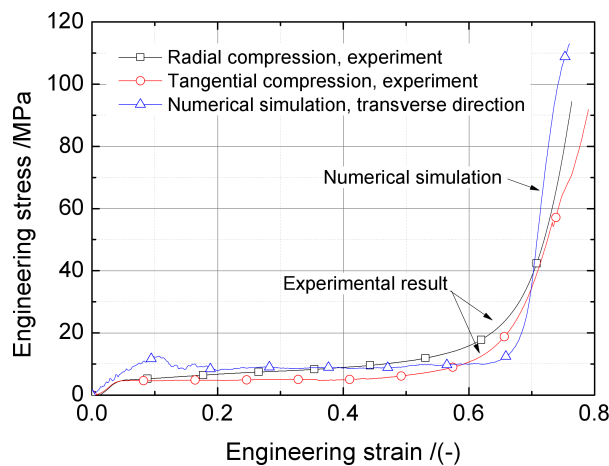
FIG. 16. Comparison of tress versus strain curves for radial, tangential and transverse compression.

4.5. Relation of plateau stress ratio and porosity

Porosity is a main influencing factor that affects the mechanical property of porous material. Ratio of plateau stress to non-porous material yield strength

is taken as an important parameter to study the porosity effect in the present numerical analysis. Taking porosity effect expression into account, relation of plateau stress ratio and porosity can be written as

$$(4.1) \qquad \sigma(\varphi) = \frac{1}{m_1\sqrt{2\pi}} e^{-m_2 \left(\frac{\varphi}{m_1}\right)^2},$$

where φ is the material porosity and the parameters m_1 and m_2 are constants. For non-porous structure, the stress level is given as 317 MPa using Multi-scale simulation method [13]. For a plateau stress equal to 30 MPa under axial compression and based on the definition in Eq. (4.1), the relation of stress ratio and porosity for axial compression is written as:

$$(4.2) \qquad \sigma(\varphi) = \frac{1}{0.398942\sqrt{2\pi}} e^{-0.698968 \left(\frac{\varphi}{0.398942}\right)^2} \implies \sigma(\varphi) = e^{-4.391744\,\varphi^2}.$$

For transverse compression, plateau stress is about 10 MPa. Expression of stress ratio versus porosity for transverse compression is written as:

$$(4.3) \qquad \sigma(\varphi) = \frac{1}{0.398942\sqrt{2\pi}} e^{-1.024644 \left(\frac{\varphi}{0.398942}\right)^2} \implies \sigma(\varphi) = e^{-6.438151\,\varphi^2}.$$

Based on equation (4.2) and (4.3), plateau stress ratio versus porosity curves are plotted as shown in Fig. 17. A slight difference between axial and transverse compression conditions was observed. Results indicate that plateau stress ratio decreases sharply as porosity increases up to 80%. This indicates that porosity affects the material plateau stress greatly when the material has a small porosity. The decreasing rate of plateau stress ratio becomes very slow when porosity is over 0.8.
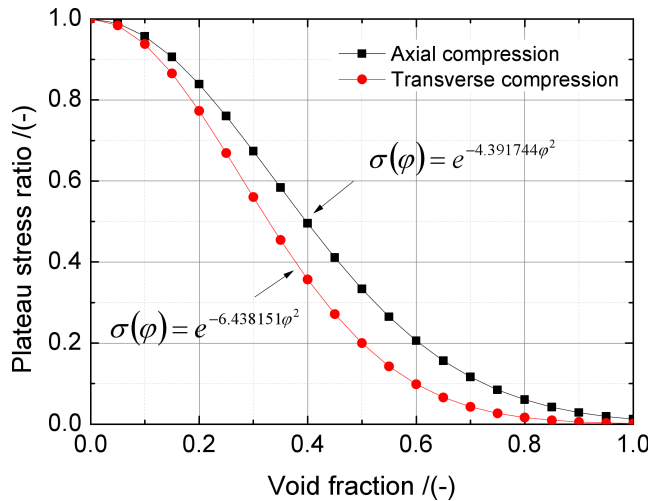
FIG. 17. Plateau stress ratio versus porosity curve in axial and transverse direction compression.

5. MODEL POROSITY AND HOLE SHAPE EFFECT
ON MECHANICAL BEHAVIOR

5.1. *Relation of microstructure porosity and wood mechanical property*

Additional finite element simulations are performed in the present work to discuss the influence of wood porosity on the mechanical properties of wood. For this purpose, six numerical models with different porosity are developed. The RVE model sizes are the same with a cubic side equal to 495 μm and six porosities equal to 0, 0.09, 0.33, 0.51, 0.73 and 0.89. The models are uniaxially compressed by rigid bodies in the wood axial direction. Stress versus strain curves of different porosity models are shown in Fig. 18. It indicates that initial yield strength decreases as the porosity increasing. Stress plateau is clear for stress strain curves of high porosity models. For low porosity models, stress strain curve is similar to the elastic-plastic deformation behavior for a metal.
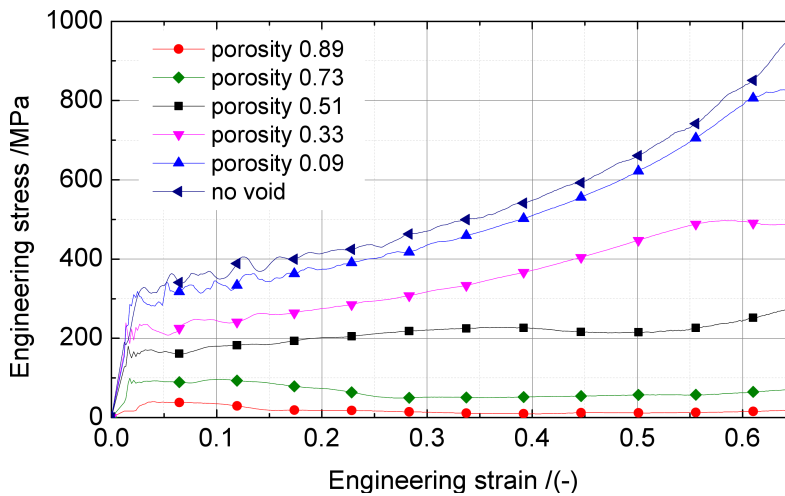
FIG. 18. Stress versus strain curves of different porosity structures.

In order to compare compression behavior of different porosities, three curves at fixed strain levels equal to 0.1, 0.3 and 0.5 are presented in Fig. 19. Results show that the stress level is linearly decreasing with porosity. As the porosity exceeds 0.5, the stress levels at 0.3 and 0.5 strains become identical. This indicates that stress plateau becomes stable for high porosity model, which contains enough void space, resulting in a wide stress plateau under compression loading. On the contrary, there is a smaller deformation space for low porosity model. Accordingly, stress increases slightly with strain under the compression process, which makes it difficult to find a plateau region in the stress strain curves.
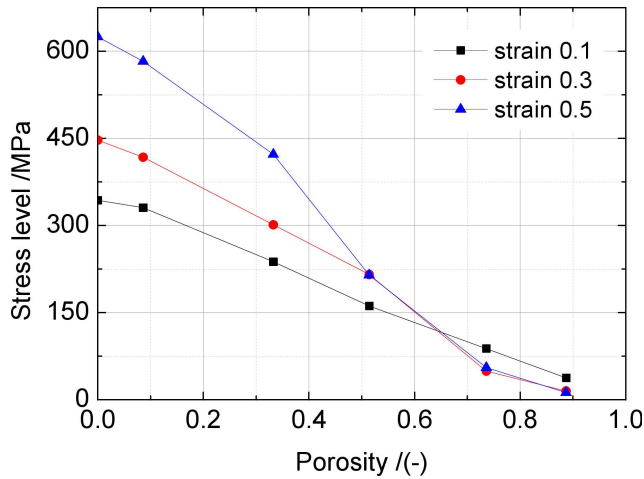
Fig. 19. Porosity effect on stress level for three different strain values.

5.2. Hole shape effect on wood axial compression mechanical property

In the previous simulations, wood microstructure with hexagon holes was analyzed. In order to discuss the effect of hole shape on wood's mechanical properties, three additional RVE models of circle, pentagon and square holes are simulated. Dimensions of the microstructures are shown in Fig. 20. Porosities of circle, pentagon and square models are equal to 0.66, 0.38 and 0.64 respectively.
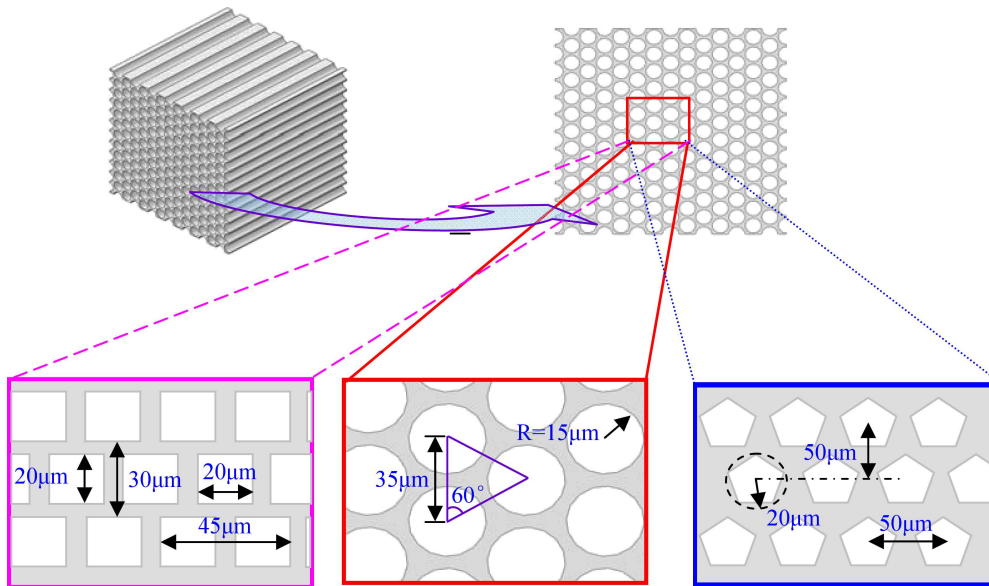
Fig. 20. Dimensions of microstructures based on different shape holes.

Figure 21 shows the stress strain curves under compression process for three different hole shapes. Results indicate that the hole shape has a clear effect on the plateau stress. Although the model with circular holes has the largest porosity among the three models, its plateau stress was not the largest. The hole shape also affects the locking strain at which the model with the largest porosity has a higher locking strain value.
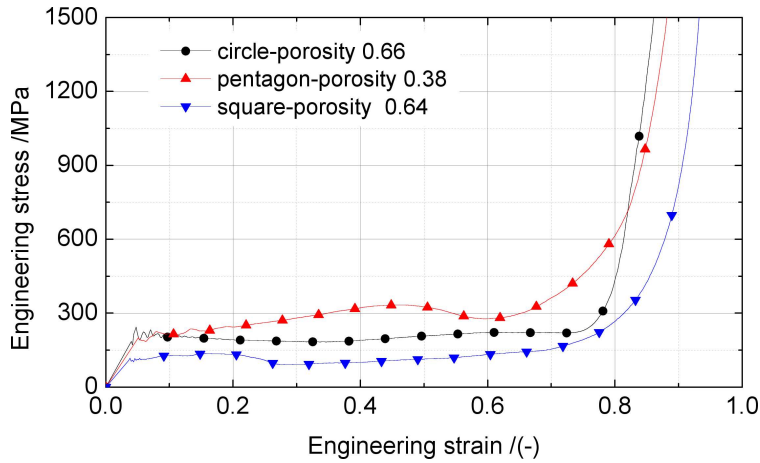
FIG. 21. Stress versus strain curves for different hole shapes.

The effect of porosity and hole shape on the stress level is also studied taking into consideration the porosity and hole shape results presented in Fig. 19 and Fig. 21, respectively. FE simulation results show that the circle hole model has the highest stress level at a certain strain as shown in Fig. 22. Because the
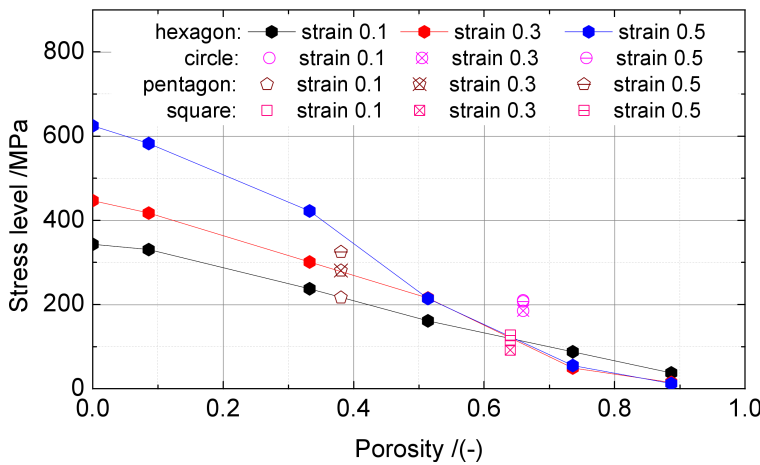
FIG. 22. Hole shape and porosity effect on stress level.

corners of hexagon, pentagon and square holes induce stress concentration in compression process, their stress levels are smaller than that of circle-hole model. Besides porosity effect on wood behavior, hole shape is also an important factor in wood microstructure numerical simulation. Thus, a good RVE model for wood should be constructed according to scanning electron microscope observation results.

6. Conclusions

Spruce compression experiments under axial, radial and tangential loadings are performed in the present work. The main failure modes observed during the experiments under axial compression are fiber buckling and wrinkle. On the other hand, fiber slippage and delamination occur when the wood specimen is loaded under radial or tangential direction. Spruce axial compressive yield strength is much higher than that of radial and tangential compressions. Radial and tangential compressive yield strengths are almost identical. Energy absorption efficiency and ideality energy absorption efficiency in different loading directions are analyzed. For certain deformation condition, energy absorption efficiency under axial loading is larger than that under radial and tangential directions. Ideality energy absorption efficiency along radial or tangential direction is larger than that of axial. The stress strain curves predicted using the RVE models agree well with experimental results. Wood micro-cell arrangement pattern results in macromechanical property anisotropy. Porosity and hole shape have strong effect on the mechanical response of wood. Finally, dimension, porosity and hole shape should be considered in developing RVE numerical simulation.

Acknowledgment

References

1. Adalian C., Morlier P., *A model for the behaviour of wood under dynamic multiaxial compression*, Composites Science and Technology, **61**, 3, 403–408, 2001.

2. Trtik P., Dual J., Keunecke D. *et al.*, *3D imaging of microstructure of spruce wood*, Journal of Structural Biology, **159**, 1, 46–55, 2007.

3. GINDL W., GUPTA H.S., SCHÖBERL T., LICHTENEGGER H.C., FRATZL P., *Mechanical properties of spruce wood cell walls by nanoindentation*, Applied Physics A, **79**, 8, 2069–2073, 2004.

4. REITERER A., LICHTENEGGER H., FRATZL P. *et al.*, *Deformation and energy absorption of wood cell walls with different nanostructure under tensile loading*, Journal of Materials Science, **36**, 19, 4681–4686, 2001.

5. SONDEREGGER W., NIEMZ P., *The influence of compression failure on the bending, impact bending and tensile strength of spruce wood and the evaluation of non-destructive methods for early detection*, Holz als Roh-und Werkstoff, **62**, 5, 335–342, 2004.

6. ORSO S., WEGST U.G.K., ARZT E., *The elastic modulus of spruce wood cell wall material measured by an in situ bending technique*, Journal of Materials Science, **41**, 16, 5122–5126, 2006.

7. MACKENZIE-HELNWEIN P., MÜLLNER H.W., EBERHARDSTEINER J. *et al.*, *Analysis of layered wooden shells using an orthotropic elasto-plastic model for multi-axial loading of clear spruce wood*, Computer Methods in Applied Mechanics and Engineering, **194**, 21, 2661–2685, 2005.

8. BOONSTRA M.J., RIJSDIJK J.F., SANDER C. *et al.*, *Microstructural and physical aspects of heat treated wood*, Part 1. Softwoods, Maderas, Ciencia y Tecnología, **8**, 3, 193–208, 2006.

9. WIDEHAMMAR S., *Stress-strain relationships for spruce wood: influence of strain rate, moisture content and loading direction*, Experimental Mechanics, **44**, 1, 44–48, 2004.

10. GINDL W., *The effect of lignin on the moisture-dependent behavior of spruce wood in axial compression*, Journal of Materials Science Letters, **20**, 23, 2161–2162, 2001.

11. GONG M., SMITH I., *Effect of load type on failure mechanisms of spruce in compression parallel to grain*, Wood Science and Technology, **37**, 5, 435–445, 2004.

12. YILDIZ S., GEZER E.D., YILDIZ U.C., *Mechanical and chemical behavior of spruce wood modified by heat*, Building and Environment, **41**, 12, 1762–1766, 2006.

13. SAAVEDRA FLORES E.I., FRISWELL M.I., *Multi-scale finite element model for a new material inspired by the mechanics and structure of wood cell-walls*, Journal of the Mechanics and Physics of Solids, **60**, 7, 1296–1309, 2012.

14. VASIC S., SMITH I., LANDIS E., *Finite element techniques and models for wood fracture mechanics*, Wood Science and Technology, **39**, 1, 3–17, 2005.

15. TABIEI A., WU J., *Three-dimensional nonlinear orthotropic finite element material model for wood*, Composite Structures, **50**, 2, 143–149, 2000.

16. MACKENZIE-HELNWEIN P., EBERHARDSTEINER J., MANG H.A., *A multi-surface plasticity model for clear wood and its application to the finite element analysis of structural details*, Computational Mechanics, **31**, 1–2, 204–218, 2003.

17. TAN W., BLANTON S., BIELECH J.P., *Summer planting performance of white spruce 1+ 0 container seedlings affected by nursery short-day treatment*, New Forests, **35**, 2, 187–205, 2008.

18. ZHONG W.Z., SONG S.C., HUANG X.C. *et al.*, *Research on static and dynamic mechanical properties of spruce wood by three loading directions*, Chinese Journal of Theoretical and Applied Mechanics, **43**, 6, 1141–1150, 2011.

19. Shipsha A., Berglund L.A., *Shear coupling effects on stress and strain distributions in wood subjected to transverse compression*, Composites Science and Technology, **67**, 7, 1362–1369, 2007.

20. Rusinek A., Zaera R., Forquin P. *et al.*, *Effect of plastic deformation and boundary conditions combined with elastic wave propagation on the collapse site of a crash box*, Thin-Walled Structures, **46**, 10, 1143–1163, 2008.

21. Keskin H., Atar M., Togay A., *Impacts of impregnation with Imersol-Aqua on the compression strength of some solid wood materials*, Construction and Building Materials, **22**, 7, 1402–1408, 2008.

22. Miltz J., Gruenbaum G., *Evaluation of cushioning properties of plastic foams from compressive measurements*, Polymer Engineering & Science, **21**, 15, 1010–1014, 1981.

23. Smith I., Landis E., Gong M., *Fracture and Fatigue in Wood*, John Wiley and Sons: Chichester, UK, 2003.